Supplemental Information
Molecular Cell, *Volume 42*

Iwr1 Directs RNA Polymerase II Nuclear Import

Elmar Czeko, Martin Seizl, Christian Augsberger, Thorsten Mielke, and Patrick Cramer

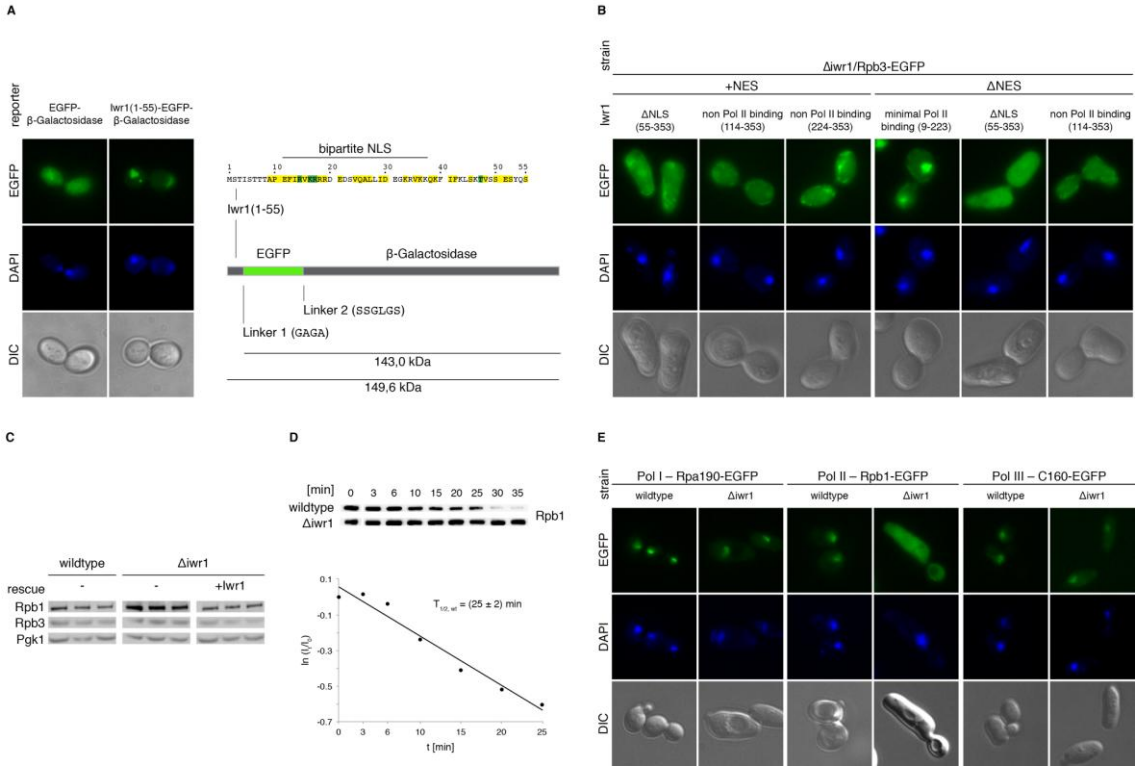

Figure S1, Related to Figure 1.

(A) Plasmid-based nuclear localization reporter with an EGFP-β-Galactosidase fusion protein. Localization of the indicated heterologous reporter protein with or without the Iwr1 bipartite NLS in wild-type yeast cells (left). Nuclear staining with DAPI (4',6'-diamidino-2-phenylindole). DIC, differential interference contrast. Schematic representation of the fusion proteins (right). Length of components is to relative size in number of amino acids. The sequence from Iwr1 fused to the reporter is indicated (invariant residues in green, residues with ≥80% conservation in yellow, compare to Figure 1A). Linker sequences were added between the three components as depicted.
(B) Localization of Pol II in Δiwr1/Rpb3-EGFP cells expressing the indicated Iwr1 truncated variants with or without NES. Nuclear staining with DAPI (4',6'-diamidino-2-phenylindole). DIC, differential interference contrast. (C and D) Protein levels of Rpb1 and Rpb3 and half-life of Rpb1 in wild-type and Δiwr1 cells.
(C) Western blot detection of Rpb1 (8WG16), Rpb3 and Pgk1 levels (control) in wild-type and Δiwr1 cells with or without a transformed IWR1 rescue plasmid. Triplicates from independent alkaline lysis reactions are shown.
(D) Protein half-life determination of Rpb1 in wild-type and Δiwr1 cells (top). Cycloheximide chase for the determination of the Rpb1 half-life in wild-type and Δiwr1 cells with Rpb1 (8WG16) detected by western blot. Time points after the addition of cycloheximide are indicated. Quantification of wild-type band intensity and derived Rpb1 half-life (bottom). Intensities (I) are normalized to the intensity at time point zero

(I_0). Time points outside of the linear range of the antibody are not considered. The standard error of the linear regression is indicated. For Δiwr1 cells no Rpb1 half-life was calculated, as the protein appeared stable over the course of the measurement. (E) Localization of Pol I, II and III largest subunits Rpa190-EGFP, Rpb1-EGFP and C160-EGFP, respectively, in cells with and without IWR1. Nuclear staining with DAPI (4',6'-diamidino-2-phenylindole). DIC, differential interference contrast.

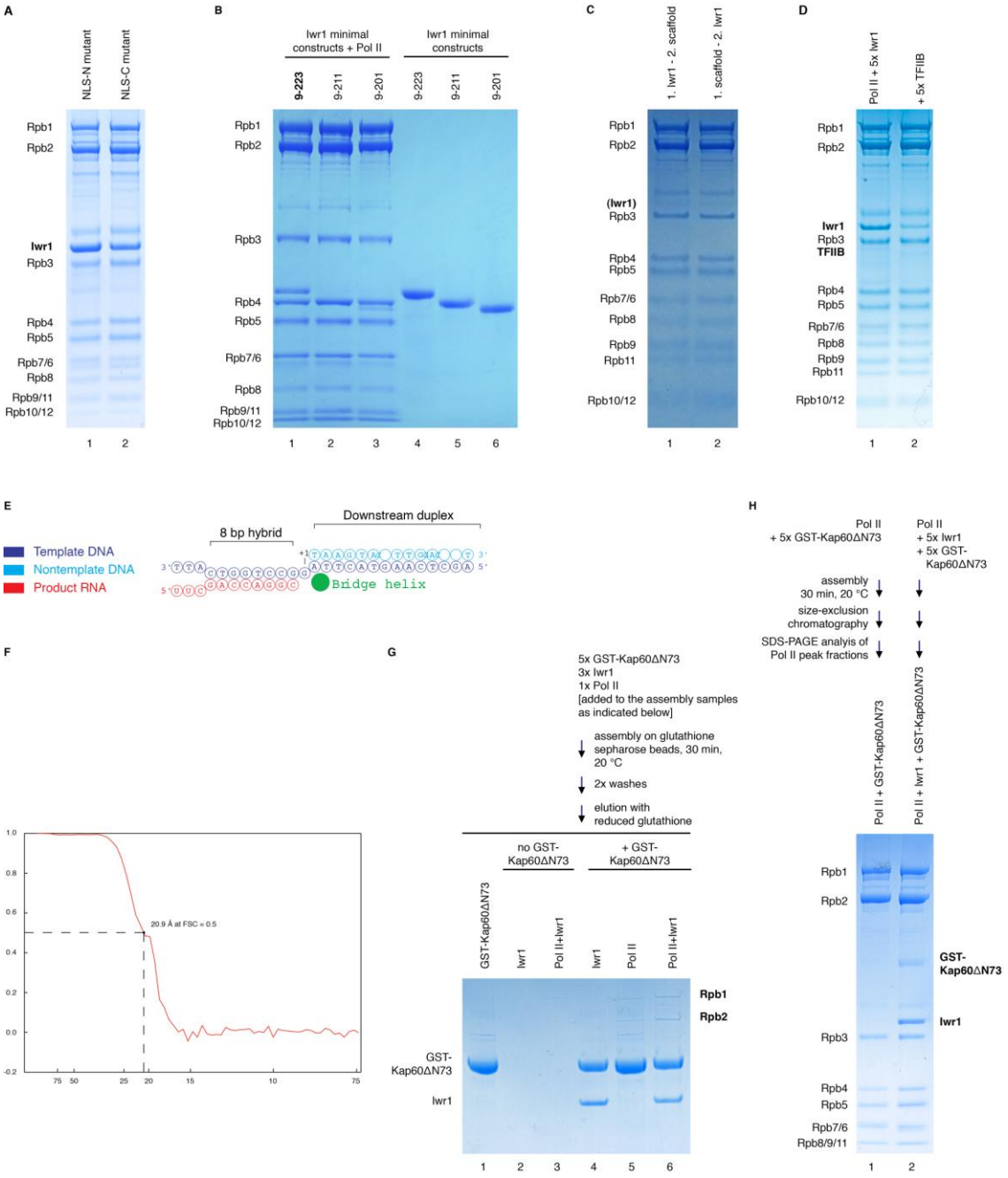

Figure S2, Related to Figure 2. Assemblies of Iwr1 Variants with Pol II and Competition with a Minimal DNA/RNA Scaffold or TFIIB; Coomassie-Stained SDS-PAGEs after Size-Exclusion Chromatography (A–D and H)

(A) Assembly of Pol II with Iwr1 NLS-mutants N and C.
(B) Determination of minimal Pol II binding constructs. Assemblies with Pol II (lanes 1-3) and purified recombinant Iwr1 variants (lanes 4-6). Iwr1 (9-223) binds stoichiometrically (defined as the minimal Pol II binding region); Iwr1 (9-211) binds, yet stoichiometry cannot be determined due to an overlap of the respective band with Rpb4; Iwr1 (9-201) binds substoichiometrically.

(C) Competition of Iwr1 and a minimal DNA/RNA scaffold for binding to Pol II. Either Iwr1 (5-fold excess) was pre-incubated with Pol II for 20 min and then the DNA/RNA scaffold (2-fold excess) was added for 20 min (lane 1) or vice versa (lane 2). The binding of DNA/RNA to Pol II was detected by the increased absorption at 260 nm in the Pol II size-exclusion chromatography peak.
(D) Competition of Iwr1 and TFIIB for binding to Pol II. Iwr1 (5-fold excess) was incubated with Pol II for 20 min (lane 1). TFIIB (5-fold excess) was additionally added for 20 min (lane 2).
(E) The minimal DNA/RNA scaffold used in (C). The bridge helix indicates the position at which the scaffold is located when bound to Pol II (Damsma et al., 2007).
(F) Fourier shell correlation (FSC) curve of the Pol II-Iwr1 cryo EM map. The resolution at 0.5 is indicated.
(G and H) Formation of a trimeric complex between Pol II-Iwr1 and GST-Kap60ΔN73. In each case the relative stoichiometric ratio between the proteins and the sequential steps during the experiment are indicated. Pull-down experiments on glutathione sepharose beads (G); Coomassie-stained SDS-PAGE. Analysis of Pol II peak fractions after size-exclusion chromatography (H).

Supplemental Tables

Table S1. Significantly differentially expressed genes (absolute $\log_2$ fold-change ≥ 1, p-value < 0.05). The 20 most strongly up- and downregulated genes out of 794 are shown representatively.

Upregulated (316 total, 40%)			**Downregulated (478 total, 60%)**		
ORF	Gene name	$\log_2$ fold-change	ORF	Gene name	$\log_2$ fold-change
YLR343W	GAS2	6,96	YGL089C	MF(ALPHA)2	-9,88
YKR046C	PET10	6,39	YER011W	TIR1	-9,77
YDR216W	ADR1	6,01	YAR071W	PHO11	-9,67
YOL058W	ARG1	5,89	YDR534C	FIT1	-8,49
YKL109W	HAP4	5,88	YBR093C	PHO5	-8,43
YFL014W	HSP12	4,83	YHR216W	IMD2	-8,36
YKR039W	GAP1	4,81	YHR136C	SPL2	-8,12
YJL088W	ARG3	4,70	YCL064C	CHA1	-8,02
YEL011W	GLC3	4,39	YDR033W	MRH1	-7,58
YKL161C	YKL161C	4,32	YAR068W	YAR068W	-7,52
YLR142W	PUT1	4,24	YAR073W	IMD1	-7,02
YER081W	SER3	3,94	YLR231C	BNA5	-6,86
YJL102W	MEF2	3,93	YJR025C	BNA1	-6,82
YPL152W	RRD2	3,84	YDL115C	IWR1	-6,13
YKR091W	SRL3	3,82	YHL047C	ARN2	-6,11
YDR042C	YDR042C	3,76	YCL027W	FUS1	-6,07
YPR002W	PDH1	3,73	YJL157C	FAR1	-6,02
YOR065W	CYT1	3,51	YIL011W	TIR3	-6,01
YDL181W	INH1	3,45	YLR136C	TIS11	-5,77
YBR230W-A	YBR230W-A	3,42	YOR009W	TIR4	-5,76

Table S2. Classification of significantly differentially expressed genes to general biological processes according to the Super GO-Slim: Process of the SGD Gene Ontology Slim Mapper.

GOID	**GO term**	**Frequency (out of 794)**		**Genome Frequency (out of 6310)**	
		[total]	[%]	[total]	[%]
9987	cellular process	549	69.1	4835	76.6
8152	metabolic process	412	51.9	3595	57.0
8150	biological process unknown	198	24.9	1247	19.8
6810	transport	127	16.0	1034	16.4
6350	transcription	87	11.0	610	9.7
7049	cell cycle	57	7.2	521	8.3
6520	cellular amino acid metabolic process	41	5.2	207	3.3
23046	signaling process	33	4.2	239	3.8
-	other	7	0.9		
-	not yet annotated	4	0.5		

Supplemental Experimental Procedures

Strains and Constructs

All yeast strains had a BY background. Deletion of IWR1 was achieved by homologous recombination at the IWR1 locus after transforming a kanMX marker (Janke et al., 2004) flanked by 50 bp homologous sequences into wild-type yeast and selecting for G418 resistance. The C-terminal EGFP fusion in frame with the Rpb1, Rpb3, Rpa190, and C160 ORF, respectively, was introduced into both the Δiwr1 and wild-type strain by homologous recombination using a cassette containing the EGFP gene and a HIS-marker (Janke et al., 2004) flanked by 50 bp homologous sequences and selecting for prototrophy on synthetic complete (SC) -HIS plates. Strain identity was confirmed by PCR. The full-length *S. cerevisiae* IWR1 gene was PCR-amplified from yeast genomic DNA with promoter regions about 500 base pairs (bp) upstream and terminator regions 250 bp downstream, and cloned into the pRS316 plasmid via *Xba*I and *Xho*I restriction sites. The NES deletion and NLS point mutations were introduced by site-directed mutagenesis or two-step PCR. The full-length ORF of the yeast IWR1 gene on the pRS316 plasmid was exchanged for truncated variants or the human homologue (ordered as a synthetic gene, Mr. Gene) by homologous recombination. The EGFP-tagged IWR1 variants were derived from the available plasmids by homologous recombination. For the NLS reporter assay about 430 bp of the ACT1 promoter region, a part of the IWR1 ORF encoding the first 55 a. a. (omitted for control), EGFP and *E. coli* lacZ were cloned in tandem into a pRS315 plasmid by a combination of restriction site cloning and homologous recombination in yeast.

Purification of Full-Length Iwr1 and Truncation Variants

IWR1 constructs were cloned into a pET21b vector via *Nde*I and *Xho*I restriction sites. *E. coli* BL21 (DE3) RIL cells (Stratagene) were transformed with plasmids and grown in LB medium at 37° C to an OD_{600} of 0.5. Expression was induced with 0.5 mM IPTG for 16 h at 18 °C. Cells were lysed by sonication in buffer A (20 mM Tris pH 8.0, 150 mM NaCl, 10 mM β-mercaptoethanol). After centrifugation, imidazole was added to a final concentration of 10 mM to the supernatant and loaded onto a 1 ml Ni-NTA column (Qiagen) equilibrated with buffer A containing 10 mM imidazole. The column was washed three times with 20 column volumes (CVs) of buffer A containing 20, 30, or 40 mM imidazole, and eluted with buffer A containing 250 mM imidazole. Proteins were purified by anion exchange chromatography (Mono Q). The column was equilibrated with buffer B (20 mM Tris pH 8.0, 100 mM NaCl, 10 mM β-mercaptoethanol), and proteins were eluted with a linear gradient of 20 CVs from 100 mM to 1 M NaCl in buffer B. After concentration, the sample was applied to a Superose 12 size exclusion column (GE Healthcare) equilibrated with Pol II buffer (5 mM Hepes pH 7.25, 40 mM ammonium sulphate, 10 μM $ZnCl_2$, 10 mM DTT). Protein was concentrated to 2 mg/ml and flash-frozen in liquid nitrogen.

Cryo-Electron Microscopic Structure Determination

Assembled Pol II-Iwr1 complexes were concentrated to 0.1 mg/ml and applied to glow-discharged carbon coated holey grids (Quantifoil R3/3 + 2 nm Carbon on top). Cryo samples were flash-frozen in liquid ethane using a semi-automated controlled-environment system (Vitrobot, FEI Company) at 4° C, 95% humidity, and stored in liquid nitrogen until transfer to the microscope. Micrographs were recorded with a low

dose of 25 electrons/Å^2 on a Tecnai Polara F30 field emission gun microscope at 300 kV at underfocus values in the range of 1.5-3.5 µm and scanned on a Heidelberg drum scanner with a pixel size of 1.23 Å on the object scale. The contrast transfer function was determined using CTFFIND and SPIDER (Frank et al., 1996). Particles were picked automatically with SIGNATURE (Chen and Grigorieff, 2007) and were then sorted visually. The data was processed using SPIDER (Frank et al., 1996). Initially 47617 particles from 35 micrographs were aligned using as a reference the complete Pol II structure (PDB code 1WCM) (Armache et al., 2005) that was filtered to 25 Å resolution. After the first 20 rounds of angular refinement particles were sorted against the initial reference filtered to 22.5 Å resolution for five more rounds. Sorting resulted in a volume based on 25206 particles showing a significant difference density in the Pol II cleft and 22411 particles being assigned to the initial reference. Also a significant positive difference density appeared next to the Rpb4/7 region that was complemented by a negative difference density on the other side of Rpb4/7. This implied a shift of this region relative to the position in the crystal structure and substantiated that the map was free of reference bias and represented experimental data. The images were backprojected in real space using the refined angles. The resulting reconstruction was Butterworth low-pass filtered to 22.5 Å and used as a reference for another round of alignment and refinement as above. This procedure was iterated until no changes in growth of additional densities were observed. Finally, a 20.9 Å reconstruction of Pol II-Iwr1 was obtained (Figure 2A). A final difference density was calculated by subtracting the reference filtered to the same resolution from the Pol II-Iwr1 reconstruction using normalized maps. Additionally, a difference density with a reconstruction of Pol II by itself was calculated which was in agreement with the location of the major difference density derived by the prior analysis. Although this difference density was larger, interpretation was complicated by the presence of higher noise levels. The resolution for the final volume was estimated based on a cutoff value of 0.5 for the Fourier shell correlation (Supplemental Figure 3). Negative-stain samples were treated with 2% (w/v) uranyl acetate and subsequently dried at room temperature. Images were recorded on a FEI Tecnai Spirit microscope operating at 120 kV, equipped with a LaB_6.filament and a 2k x 2k FEI Eagle CCD camera at a magnification of 90.000.

Supplemental References

Armache, K.-J., Mitterweger, S., Meinhart, A., and Cramer, P. (2005). Structures of complete RNA polymerase II and its subcomplex Rpb4/7. J Biol Chem *280*, 7131-7134.

Chen, J.Z., and Grigorieff, N. (2007). SIGNATURE: a single-particle selection system for molecular electron microscopy. J Struct Biol *157*, 168-173.

Damsma, G.E., Alt, A., Brueckner, F., Carell, T., and Cramer, P. (2007). Mechanism of transcriptional stalling at cisplatin-damaged DNA. Nat Struct Mol Biol *14*, 1127-1133.

Frank, J., Radermacher, M., Penczek, P., Zhu, J., Li, Y., Ladjadj, M., and Leith, A. (1996). SPIDER and WEB: processing and visualization of images in 3D electron microscopy and related fields. J Struct Biol *116*, 190-199.

Janke, C., Magiera, M.M., Rathfelder, N., Taxis, C., Reber, S., Maekawa, H., Moreno-Borchart, A., Doenges, G., Schwob, E., Schiebel, E.*, et al.* (2004). A versatile toolbox for PCR-based tagging of yeast genes: new fluorescent proteins, more markers and promoter substitution cassettes. Yeast *21*, 947-962.